DOI: 10.1002/ ((please add manuscript number))
Article type: Full Paper

Evidences of the Effect of GO and rGO in PCL Membranes on the Differentiation and Maturation of Human Neural Progenitor Cells

Sandra Sánchez-González, Nazely Diban, Fabio Bianchi, Hua Ye, Ane Urtiaga*

———

S. Sánchez-González, Dr. N. Diban, Prof. A. Urtiaga
Department of Chemical and Biomolecular Engineering, University of Cantabria
Avda. Los Castros s/n, 39005 Santander, Spain
E-mail: *dibann@unican.es*

F. Bianchi, Dr. H. Ye
Institute of Biomedical Engineering (IBME), Department of Engineering Science, University of Oxford
Oxford OX3 7DQ, UK

———

The effect of doping graphene oxide (GO) and reduced graphene oxide (rGO) into poly(ε-caprolactone) (PCL) membranes prepared by solvent induced phase separation (SIPS) is evaluated in terms of nanomaterial distribution and compatibility with neural stem cell growth and functional differentiation. Raman spectra analyses demonstrate the homogeneous distribution of GO on the membrane surface while rGO concentration increases gradually towards the center of the membrane thickness. This behavior is associated with electrostatic repulsion that PCL exerted towards the polar GO and its affinity for the non-polar rGO. In vitro cell studies using human induced pluripotent cells derived neural progenitor cells (NPCs) show that rGO increases marker expression of NPCs differentiation respect to GO and significantly to tissue culture plate (TCP). Moreover, the distinctive nanomaterials distribution defines the cell-to-nanomaterial interaction on the PCL membranes thereby affecting NPC maturation to functional neurons. GO nanomaterials on the membrane surface favor higher number of active matured neurons, while PCL/rGO membranes present cells with significantly higher magnitude of neural activity compared to TCP and PCL/GO despite there is no direct contact of rGO with the cells on the membrane surface. Overall, this work evidences the important role of electrical properties of the rGO nanomaterials on the stimulation of neural cell electro-activity on PCL membrane scaffolds.

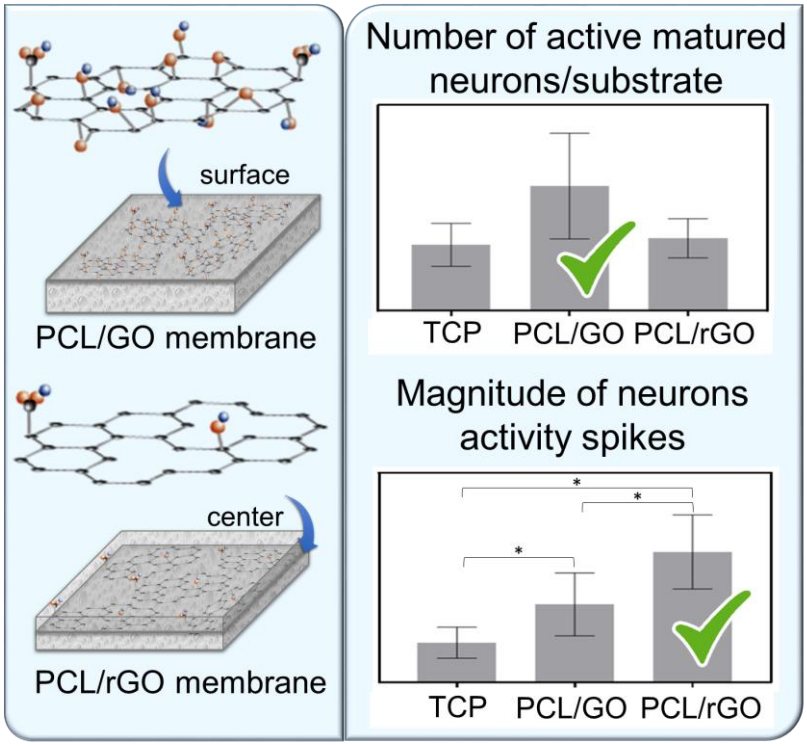
surface
PCL/GO membrane
center
PCL/rGO membrane
Number of active matured neurons/substrate
TCP
PCL/GO
PCL/rGO
Magnitude of neurons activity spikes
*
*
*
TCP
PCL/GO
PCL/rGO

1. Introduction

The investigation of human neural networks as *in vitro* models could provide knowledge about brain functionalities, neurodegenerative disorders, and a platform for drug discovery and testing.[1] The development of human neural cell models is progressing due to the recent advances in the derivation of neurons from human stem cells, which includes induced pluripotent cells (iPSC), mesenchymal stem cells (MSCs) and embryonic stem cells (ESCs).[2] However, the regeneration of functional central nervous system (CNS) is still one of the major challenges in regenerative medicine. Among the current approaches to improve the capacity of *in vitro* regeneration of neural cells is the use of biomaterials, such as synthetic polyesters, which has been demonstrated to support neural cell growth and regeneration.[3,4]

Lately, graphene and its derivatives have been considered promising candidates to facilitate neural differentiation of human stem cells and to form neuronal fibers for neural tissue engineering applications.[5,6] However, the potential cytotoxicity [7] and the pursuit of biodegradable and bioresorbable materials [8] questions the use of graphene and graphene derivatives as scaffolds for biomedical applications. Moreover, since single biomaterials have drawbacks in mimicking the properties of native tissue, the use of composite graphene/biomaterial scaffolds is becoming increasingly common.[9,10]

Composites of biocompatible and bioresorbable polymers, e.g. poly(ε-caprolactone) (PCL), and graphene based nanomaterials, have been shown as promising substrates for tissue engineering applications.[11] PCL is a bioresorbable and biocompatible polyester with a large list of FDA approved biomedical devices [12] that can help mitigate the cytocompatibility and resorbability problems associated with graphene-based nanomaterials. The introduction of graphene nanomaterials reinforces the polymer matrix, and may contribute to enhance the electrical properties of the polymer-graphene composites, thus stimulating neural cell differentiation for neural tissue engineering.[10,13] For example, Song et al.[14] studied the effect of graphene oxide (GO) loading on electrospun PCL nanofibers. Low concentrations of

GO addition to the PCL matrix (0.3-0.5%) showed suitable cell adhesion characteristics and differentiation of rat pheochromocytoma (PC12-L), due to the surface oxygenated groups and increased conductivity of GO with respect to plain PCL. GO loadings of 1 wt% caused clusters with negative effects on cell behaviors. In our previous work,[15] we developed composites of PCL with GO and reduced graphene oxide (rGO) by solvent induce phase separation (SIPS) that showed promising properties and neural cell biocompatibility to be used in perfusion bioreactors for *in vitro* neural models. Moreover, the study of degradation products and the permanence of the nanomaterials in the polymeric matrix during the hydrolysis of the polymer indicates low cytotoxic effects.[16]

The application of different external stimuli, such as electrical, pulsed laser, flash photo, chemical and patterning stimulations, have reported favorable stem cell differentiation on graphene-based scaffolds.[17] Besides to external stimulations, also intrinsic properties, such as surface chemistry and nanomorphology, of the graphene-based nanomaterials can create specific cell-substrate interactions that improves cell differentiation. This type of materials-based stimulation is particularly interesting because the use of external and, in some cases invasive, equipments to trigger stem cell differentiation can be avoided in clinical and/or tissue engineering settings. Previous works have reported that the response of cells in terms of adherence, proliferation and differentiation was affected by the type of graphene-based nanomaterial used. For instance, Akhavan et al.[18] compared the effect of self-supported GO and rGO scaffolds on the proliferation and differentiation of human neural stem cells (hNSCs). The better hydrophilicity of GO compared to rGO led to a higher proliferation on GO scaffolds. Neural cell differentiation was improved on rGO, attributed to the better electrical conductivity. Studies comparing the presence of GO or rGO in other polymeric membranes for neural tissue engineering [14,19–21] have shown that graphene based nanomaterials significantly promote cell cultures in terms of cell proliferation and/or differentiation. However, to the best of our knowledge, the effect of doping PCL membranes

with GO or rGO on hNSC differentiation and maturation has not been investigated so far. Moreover, it is expected that during the fabrication of the PCL/graphene-based membranes using SIPS, the different chemistry and hydrophilicity of the GO and rGO nanomaterials will produce different affinity towards the non-polar polymer matrix and the polar solvent (alcohol) used as coagulant. Similarly, we are not aware of previous works that analyzed the effect of the nanomaterial polarity on their dispersability and distribution in the polymer matrix of the scaffold by SIPS. We hypothesize that our polymer-graphene composite scaffolds will procure different micro-environmental cues, depending on the nanomaterials distribution on the PCL matrix and their chemical structure that will affect stem-cell fate and neural differentiation, maturation and ultimately synaptic function.

In order to cover the lack of data reported above, the aim of this work was to evaluate the effect of GO and rGO loadings in the PCL membranes fabricated by SIPS, through chemical and electrical characterization, and by evaluating suitability for human iPSC-derived neural progenitor cells (NPCs) culture. The influence of nanomaterials chemistry on their distribution into the PCL matrix was characterised via Raman spectroscopy, contact angle measurements and conductivity. At the cellular level, culture analyses were performed to evaluate the differentiation of NPCs into functional mature neurons. Cell adhesion, proliferation, differentiation and maturation were studied by morphological and immunocytochemistry analyses. Calcium imaging was used to quantify the neural activity of matured iPSC-derived neurons cultured on PCL/GO and PCL/rGO membranes.

2. Results and discussion

2.1. Membrane characterization

Figure 1a shows the Raman spectra at a specific point on the surface of the PCL, PCL/GO and PCL/rGO membranes. The spectrum showed the characteristic bands of PCL polymer.[22] The Raman bands at 1282, 1304, 1417, 1438 and 1469 cm^{-1} are attributed to CH_2 vibrations

while the ester group C=O appears at 1722 cm^{-1}. In the spectra of PCL/GO membranes in Figure 1a, the presence of the G band at 1580–1600 cm^{-1} and the D band at 1356 cm^{-1} can be clearly seen, characteristic of Raman spectrum of GO.[23,24] **Figure 1b** depicts a 400 × 340 µm mapping of the D band intensity of PCL/GO membrane surface showing that the surface of the PCL/GO membrane was uniformly covered by GO nanomaterials with a homogeneous distribution.

In the Raman spectrum of PCL/rGO membrane surfaces, neither D or G bands could be detected (Figure 1a). However, in the cross section of the PCL/rGO membranes both D and G bands were observed. **Figure 1c** plots the intensity of the D band in the cross section of the PCL/rGO membranes showing an increased concentration of rGO nanomaterial towards the center of the PCL/rGO membrane. These results demonstrate that the introduction of GO or rGO nanomaterials into the PCL matrix affected the distribution of the nanomaterials in the membrane matrix differently, during the SIPS processing. While the PCL/GO membranes showed that the nanomaterials were homogeneously dispersed on the membrane surface, rGO nanomaterials concentrated at the center of the membrane. The different nanomaterial distribution observed can be attributed to the polarity of the components during the phase inversion process; GO contains oxygenated groups that confer a polar behaviour, whilst, rGO is a non-polar nanomaterial, as the majority of the polar oxygenated groups have been reduced. The coagulation bath employed for the phase inversion consists of a polar alcohol (isopropanol), while the PCL polymer matrix is non-polar. During the phase inversion process, rGO will tend to be attracted to the material with similar polarity (PCL), while the GO nanomaterials will be atracted towards the polar coagulation bath [24] and will tend to be expelled out of the polymer matrix. This is in agreement with Xu et al.,[25] who suggested that GO nanomaterials would migrate spontaneously to the surface of a polyvinylidene fluoride polymeric membrane in order to reduce the interface energy during the phase inversion process using distilled water as coagulant.

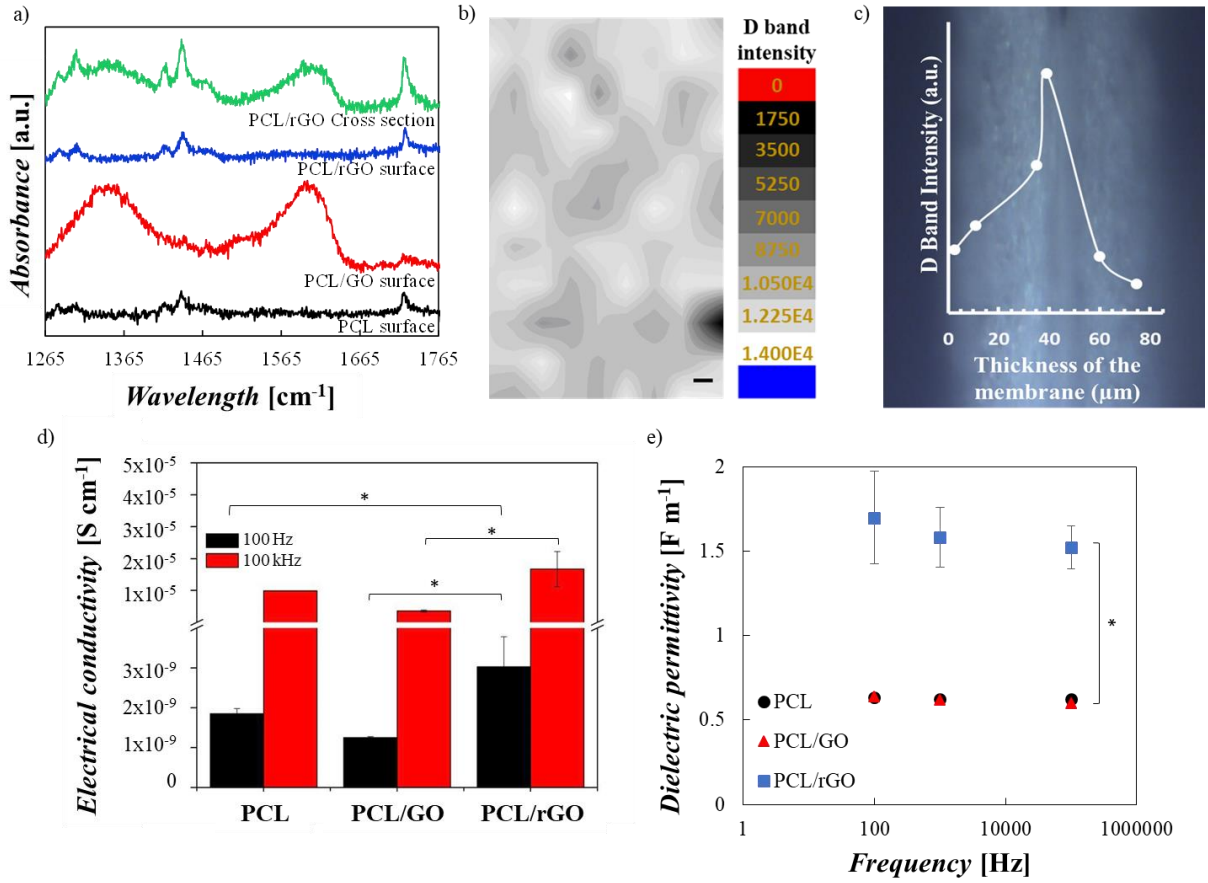

Figure 1. a) Raman spectra of the surface of the PCL and PCL/GO membranes, and the surface and cross section of the PCL/rGO membranes. b) Surface distribution of the D band intensity of GO nanomaterials on PCL/GO membranes. Scale bar= 20 µm. c) Profile of the D band intensity at different points of throughout the thickness of PCL/rGO membrane. Points correspond to singular experimental data. Lines are only for readers' guidance. d) and e) Electrical properties of the PCL, PCL/GO and PCL/rGO membranes obtained from impedance analysis, being d) electrical conductivity calculated at 100 and 100000 Hz and e) dielectric permittivity calculated at 100, 1000 and 100000 Hz. *=p>0.05 using one way ANOVA with Tukey's multiple comparison test. Dielectric constants of PCL/rGO membranes showed significant statistical difference (p>0.05) at any frequency in the range tested.

Consequently, the nanomaterial distribution on the membranes and their chemistry (polarity) also affected the water contact angle of the membranes. The water contact angles of the PCL, PCL/GO and PCL/rGO membranes were 96 ± 11˚, 72 ± 10˚ and 94 ± 4˚, respectively. The water contact angle of PCL/GO membranes was significantly different compared to PCL and PCL/rGO. PCL/GO membranes became significantly more hydrophilic as a result of the presence of polar oxigentated groups of the GO nanomaterials on the membrane surface.[26,27] rGO nanomaterials did not affect the overall PCL hydrophilicity (water contact angle) as the non-polar rGO nanomaterials were not located on the membrane surface. This is in

accordance to other works showing that composites of polymer matrix and low concentrations of rGO (up to 1 wt%) did not differ significantly in water contact angle from plain polymer.[26,28,29]

Figure 1d and e shows the electrical properties of the PCL, PCL/GO and PCL/rGO membranes, obtained through electrical impedance analysis. Figure 1d indicated the electrical conductivity of the membranes. The conductivity of PCL membrane was found to increase with the angular frequency of the AC between $1.8\pm0.1x10^{-9}$ cm^{-1} at 100 Hz to $9.9\pm0.004x10^{-6}$ cm^{-1} at 100 kHz (Figure 1d) which is a typical behaviour reported for electrical insulators.[30] Besides, some works reported a conductivity of PCL porous structures around 10^{-10} $S\cdot cm^{-1}$ [31] The PCL/GO membranes showed similar values of conductivity than PCL membranes at any frequency. On the contrary, membranes of PCL/rGO presented significantly higher conductivity respect to PCL/GO at 100 kHz and respect to PCL and PCL/GO at 100 Hz. The observed differences in the electrical properties of the membranes could be attributed to the porous structure of the membranes [32] and to the widely recognised higher conductivity of rGO compared the GO.[33,34] As PCL, PCL/GO and PCL/rGO membranes all have similar porosity and porous structure,[15] the different electrical conductivity of GO and rGO nanomaterials largely reported in the literature (i.e. electrical conductivities of 0.0206 S/m for GO and 2420 S/m for rGO determined by Stankovich et al.[33]) seems to be the main reponsible of the differences on electrical behaviour observed between PCL/GO and PCL/rGO membranes. Despite the increase in electrical conductivity observed for PCL/rGO membranes, the low percentage of nanomaterial loaded in the membranes (0.67 w/w%) was insufficient to reach the electrical percolation threshold.[28,35] Figure 1e shows the dielectric permittivity of the different membranes as a function of frequency. The dielectric permittivity was significantly higher on PCL/rGO respect to PCL and PCL/GO membranes at any frequency tested. The higher dielectric permittivity observed in PCL/rGO was associated to a higher polarizability of the membranes.[36] Furthermore, the dielectric permittivity was

independent from frequency. A constant dielectric permitivity with frequency in graphene/poly(vinylidenefluoride) composites has been previously attributed to situations where graphene loading was below the electrical percolation threshold. [36]

2.2. Proliferation, differentiation and maturation of NPCs culture

Figure 2a shows the proliferation of NPCs cultured on TCP, PCL, PCL/GO and PCL/rGO membranes at 1, 3 and 5 days. Quantitative analysis of cell proliferation was carried out by cell nuclei counting. Overall, the number of cells progresively increased over time. Cells attached properly and were homogenously distributed on the surface of the sustrate with a suitable cell morphology in all cases (**Figure S1**, Supporting information). The similar cell adhesion could be a result of using matrigel as coating, to promote NPCs adhereance (**Figure S2**, Supporting information).[37] In particular, cell adhesion on non coated PCL/GO membranes presented a slight improvement in comparison to PCL and PCL/rGO membranes, potentially attributed to the lower contact angle of those membranes. The cell density at day 1 was similar on all substrates (5.77×10^4 - 6.33×10^4 cells/ substrate). At 3 and 5 days, TCP samples showed significantly higher cell numbers, with respect to the membranes, as expected ($50 \times 10^4 \pm 9 \times 10^4$ cells/ substrate at day 3 and $90 \times 10^4 \pm 19 \times 10^4$ cells/ substrate at day 5). The high surface porosity of the membranes reported in our previous work [15] might impair cell-to-cell contact and therefore delay the cell proliferation rate in contrast to the smooth TCP surface. Comparing cell proliferation on the different membranes, PCL/GO and PCL/rGO presented slighty higher cell number at day 5 ($51 \times 10^4 \pm 9 \times 10^4$ cells/ substrate and $44 \times 10^4 \pm 6 \times 10^4$ cells/ substrate, respectively) compared to PCL ($40 \times 10^4 \pm 15 \times 10^4$ cells/ substrate). This result was consistent with the results reported by several authors.[14,20,21,26,38] For instance, PCL/graphene-based scaffolds enhanced the proliferation of human mesenchymal stem cells [26] and human adipose-derived stem cells [38] compared to plain PCL scaffolds. The high surface area, elastic modulus, the stiffness of graphene and the presence of wrinkles and ripples have been cited as possible causes of the better cell proliferation.[38]

Differentiation of NPCs cultured on TCP, PCL, PCL/GO and PCL/rGO is showed in **Figure 2b, 2c** and **2d** at day 1 and day 7. Tuj1 stained cells were quantitatively evaluated by measuring i) the percentage of Tuj1-expressing cells (Figure 2b) and ii) the average length of neurites (Figure 2c), analyzing the confocal images (Figure 2d). Qualitatively, an increase of Tuj1 expression was observed from day 1 to day 7 in all cases, confirming NPC differentiation towards neural lineage (Figure 2d). Particularly, all membranes presented higher Tuj1 expression (Figure 2b) than TCP substrates. The porous structure of the surface of the fabricated membranes [15] could provide a better platform for intra-cellular communication, migration of nutrients and cellular metabolism than TCP.[34,39] It was evident qualitatively (Figure 2d) that the introduction of rGO nanomaterials into PCL membrane promoted neurite outgrowth compared to plain PCL membranes and TCP, while GO nanomaterials produced little improvement. Quantitative analysis also indicates that PCL/rGO membranes significantly accelerated the differentiation of NPCs respect to TCP in terms of Tuj1 expression (Figure 2b) and respect to TCP, PCL and PCL/GO membranes in terms of length of neurite (Figure 2c).

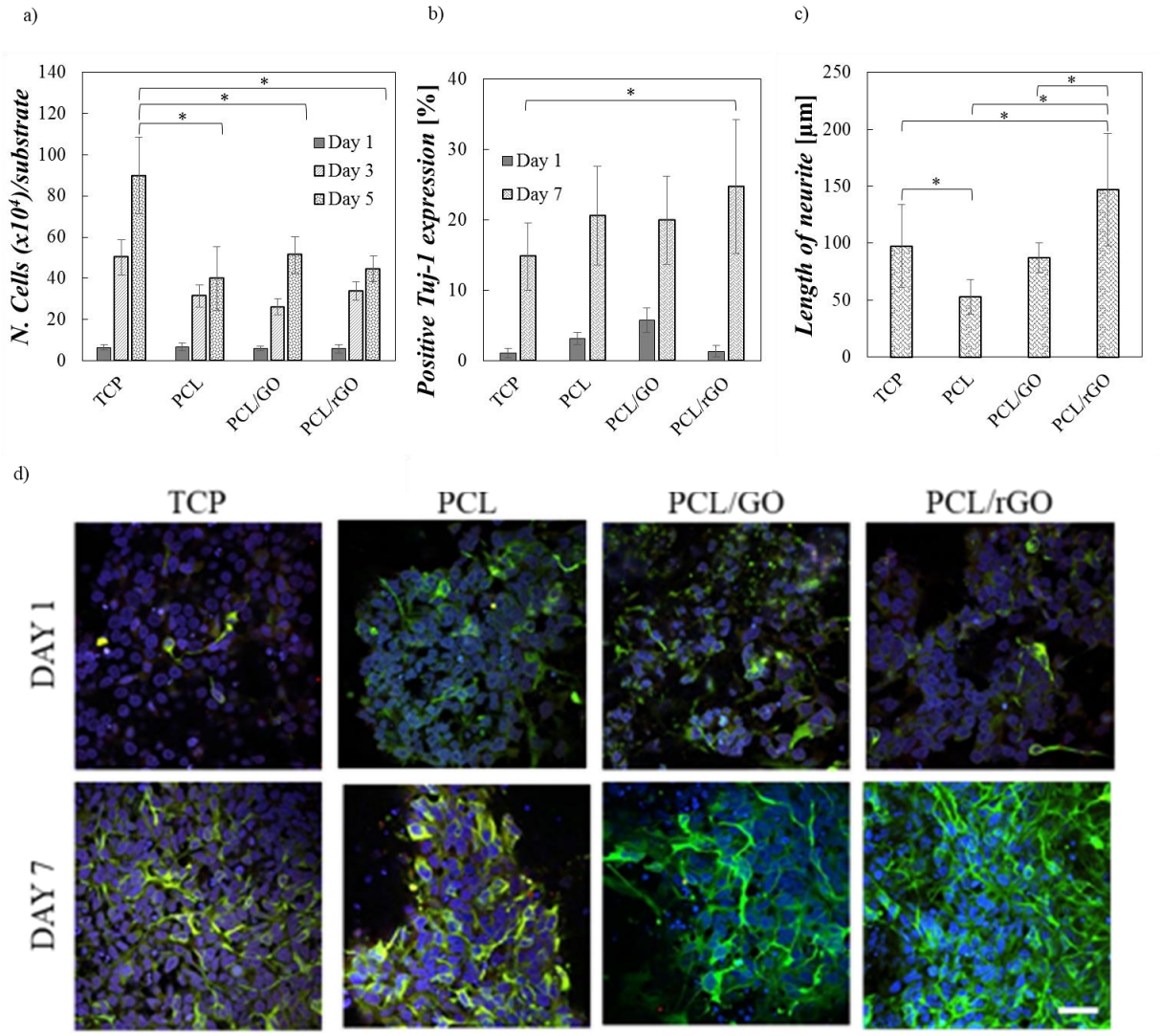

Figure 2. NPC cultured on TCP, PCL, PCL/GO and PCL/rGO membranes at a) proliferation and b), c) d) differentiation stage. a) NPC proliferation at day 1, 3 and 5. b) Differentiated NPCs at day 1 and 7 by % positive Tuj-1 expression. c) Average length of neurites of differentiated NPCs at day 7. d) Confocal microscopy images of differentiated NPCs. The microtubules of neuron cells are stained by Tuj1 (green) and the cell nuclei are counterstained by Nucblue (blue). Scale bar=50 µm. Statistical analysis was shown at day 5 for proliferation and day 7 for differentiation. *=$p<0.05$, using one-way ANOVA with Tukey's multiple comparison test.

It is known that graphene based scaffolds promote neural differentiation of hNSCs over glia differentiation, albeit the mechanism is not clear.[40] Akhavan[17] revised in the literature different possible mechanisms to rule the influence of graphene-based materials on stem cell differentiation. Those included morphological, mechanical, electrical and chemical aspects of the graphene-based nanomaterials. The mechanical properties in our PCL/graphene-based

membranes have been reported in our previous work [15] observing not significant change on the Young's Modulus that could explain any mechanical induction of stem cell differentiation. Also in that work, PCL/GO and PCL/rGO membranes presented similar membrane surface morphology, which discards topographical cues as inductive effect on cell differentiation. Regarding the surface chemistry influence of GO and rGO nanomaterials on the present membranes, the phase inversion technique allowed the selective location of the nanomaterials either on the surface in case of GO or in the membrane matrix for rGO. This segregation let us deem that the intrinsic chemistry of nanomaterials had lower effect on the better NPC differentiation and neural activity at maturation, as in PCL/rGO membranes direct cell-nanomaterial interaction was not favored.

Therefore, the different intrinsic electrical properties of GO and rGO nanomaterials still remain as the most plausible cause to explain the differences on NPC differentiation and neural activity encountered on our PCL/graphene-based membranes. The electrical impedance data showed that PCL/rGO membranes had significantly higher conductivity (Figure 1d) respect to PCL/GO and, of course, PCL membranes. Also, PCL/rGO presented a significant increase in the dielectric permittivity (Figure 1e), which implies higher polarizability than PCL and PCL/GO membranes. These electrical properties could be associated with the π bonds present on graphene-based nanomaterials [27]. The π electron-cloud formed could interact with the hydrophobic cores of proteins via electrostatic interaction due to these conductive properties. Also, Akhavan et al.[18] observed an improved hNSCs differentiation on polydimethylsiloxane (PDMS) coated with rGO due to the improved capability for electron transfer. This would explain the higher neural differentiation and the significantly higher neurite length that was observed in PCL/rGO membranes with respect to the PCL/GO membranes.

At maturation, NPCs cultured on PCL/GO and PCL/rGO showed neural morphologies, and higher concentration of neurites with respect to PCL membranes, as shown in SEM images

(**Figure 3a**). Calcium imaging, an indirect reporter of neural electrical and synaptic function was performed to study the functional maturation of NPC-derived neurons cultured on TCP, PCL/GO and PCL/rGO membranes after 20 days (**Figure 3b** and **3c**). Quantification of calcium activity was defined by the number of active neurons respect the number of active neurons on TCP (Figure 3b), and by the magnitude of the intensity change produced once the cell shows action potential (Figure 3c). PCL/GO presented the highest number of active neurons (1.9 ± 0.8 active neurons/ active neurons on TCP) followed by PCL/rGO (1.1 ± 0.3 active neurons/ active neurons on TCP), although statistical differences between substrates were not found. However, PCL/rGO showed the highest magnitude of neuronal activity, with significant differences compared to TCP and PCL/GO (Figure 3c). The magnitude of neuron activity on PCL/GO, though lower than PCL/rGO, was also significantly higher compared to TCP.

Some reports have found that the electrical properties of graphene based nanomaterials provide ion channels or neurotransmitter-related proteins, to incite spontaneous neuron activity.[11,41,42] Park et al.[40] observed that genes related to the calcium signaling pathway were significantly upregulated when hNSCs were differentiated on graphene. We suggest that the location of nanomaterial within the membranes could influence the spontaneous activity of neural cells. GO was located on the surface of the membranes, and is therefore more accessible to neurons, and consequently might induce more activity. In contrast, rGO nanomaterials were preferentially present inside the PCL/rGO membrane thickness, and were therefore not directly in contact with the neurons, hindering the interactions between the nanomaterials and the cells. Nevertheless, the cells which successfully interacted with rGO nanomaterials reached higher spike magnitude compared to GO, that could be attributed to the conductive constitution of rGO.[41,42]

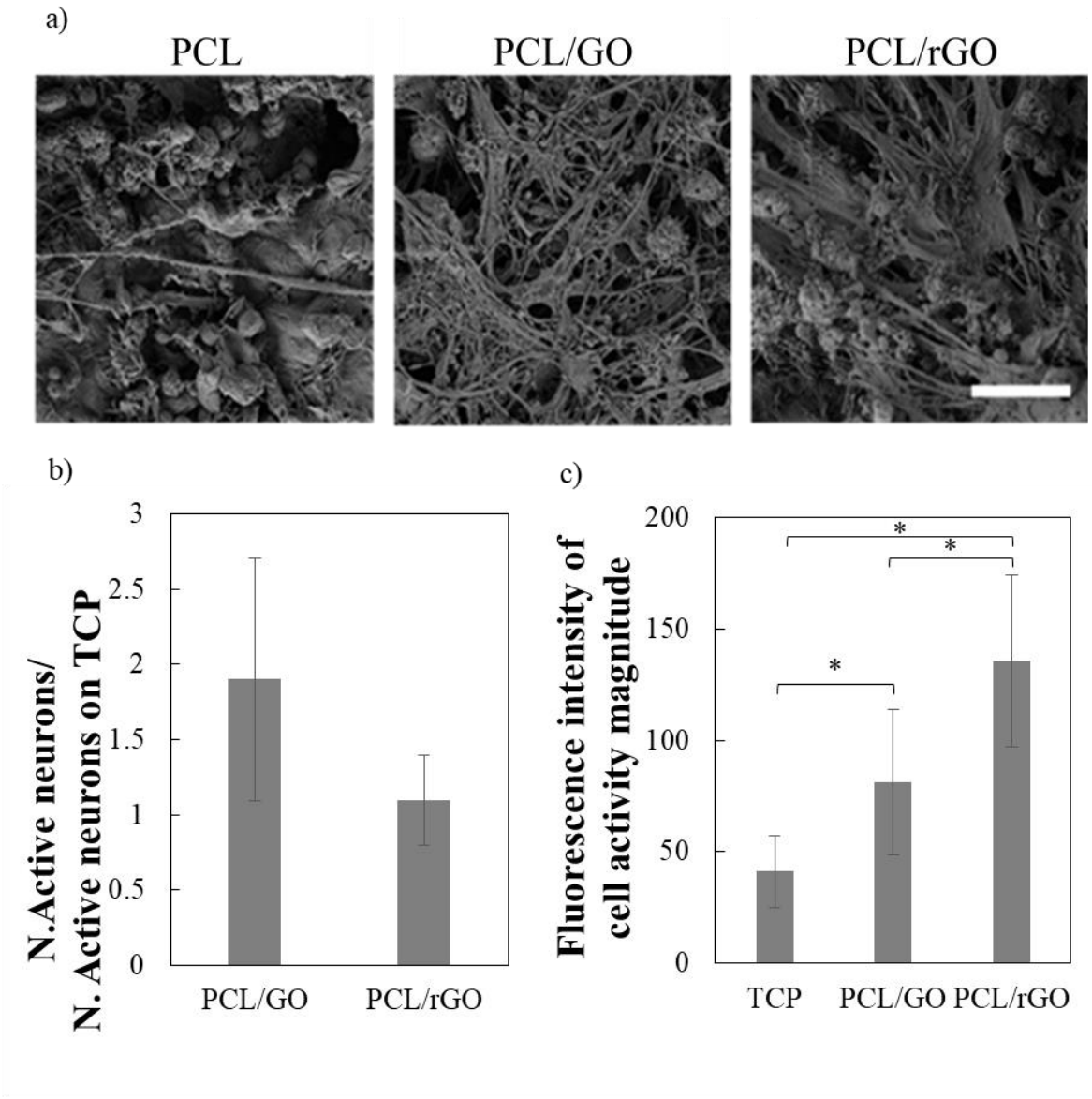

Figure 3. a) SEM images of matured neurons cultured on PCL, PCL/GO and PCL/rGO membranes after 20 days, showing extensive neurite growth. Scale bar = 10 µm. b) and c) Quantitative analysis of calcium imaging of matured NPCs cultured on TCP, PCL/GO and PCL/rGO membranes after 20 days, including b) the number of matured NPCs that fired in two minutes of recording compared to TCP (32 ± 11 active neurons/mm^2) and c) the magnitude of the matured NPCs spike. *= $p<0.05$ were calculated using one-way ANOVA with Tukey's multiple comparison test.

3. Conclusions

In the work presented here, the effect of doping poly(ε-caprolactone) (PCL) membranes fabricated by solvent induced phase separation (SIPS) with graphene oxide (GO) and reduced graphene oxide (rGO) nanomaterials has been evaluated. First, Raman spectra analysis demonstrated that during the SIPS membrane fabrication, the different polarity of GO and

rGO nanomaterials caused the GO to deposit homogeneously on the surface of the membranes while rGO concentration was found to gradually increase towards the center of the membrane thickness.

Consequently, PCL/GO membranes presented higher hydrophilicity than PCL and PCL/rGO membranes. The introduction of rGO improved significantly the electrical conductivity on PCL/rGO membranes compared to PCL and PCL/GO membranes. Adhesion and proliferation of human neural progenitor cells (NPCs) were only slightly better for PCL/GO and PCL/rGO membranes than for PCL membranes. However, the presence of GO and rGO, even in small concentrations (0.67 wt%), was shown to have a positive effect on differentiation and neural maturation of NPCs. Moreover, the distribution of the graphene-based nanomaterials on the polymer matrix had a clear influence on neural cell behavior during maturation. On one hand, the presence of GO in the PCL/GO membrane surface facilitated the direct GO-cell contact and increased the number of electrically active cells during maturation. On the other hand, neurons on PCL/rGO membranes presented significantly higher magnitude of activity spikes, attributed to the potential of rGO to induce electro-activity on neural cells.

In conclusion, despite the low nanomaterial concentrations used, NPCs cultured on PCL/GO and PCL/rGO indicated better neural cell modulation than TCP and PCL membranes. Although GO promoted higher number of active matured neurons, PCL/rGO showed the best NPCs differentiation, significantly better than PCL/GO, undoped PCL and TCP, and also demonstrated significantly higher magnitude of neural activity spikes during maturation, attributed to the better electrical properties of PCL/rGO membranes. These results lead us to consider PCL/rGO membranes as highly promising materials for scaffolds in neural tissue regeneration.

4. Experimental section

Fabrication of PCL-graphene membranes: GO and rGO were synthetized following a

modified Hummer's method as described elsewhere.[43,44] The Raman characterization of the GO and rGO nanomaterials showed that the D/G intensity ratio decreased from 0.96 for GO to 0.28 for rGO, confirming the correct reduction of GO nanomaterials. Moreover, the D/2G band intensity ratio was 0.21 and 0.24 for GO and rGO, which provided that the graphene based nanomaterials were formed by 3-4 layers.[45]

PCL/GO and PCL/rGO were fabricated using a phase inversion technique. A polymer solution containing 15 wt% PCL (MW 80 kDa, Sigma Aldrich), 0.1 wt% GO or rGO and N-methylpyrrolidone (NMP, 99% purity, Acros Organics) as organic solvent was prepared. 2-propanol (IPA, 99% purity, Oppac) was employed as coagulation bath. Detailed methodology was described in our previous work.[15] Plain PCL membranes were also prepared for comparison.

Characterization of PCL-graphene membranes: Raman spectroscopy of the different membranes was carried out with a triple spectrometer T64000 (Horiba) equipped with a confocal microscope and a Charge Coupled Device (CCD) detector (Jobin Yvon Symphony) cooled with liquid nitrogen. A 514 nm wavelength beam from a Krypton-argon ion laser was focused with a 100× objective for detection, and an effective laser power of 2mW was employed for all measurements. The count time and the number of accumulations varied depending on the sample tested. Each peak from the spectral curves was fitted using Lorentzian functions (Origin 6.0, OriginLab Corporation).

Water contact angle was measured on dry membranes to determine wettability. A drop of ultrapure water was carefully deposited with a syringe on the surface of the membrane and images were taken immediately. Water contact angle was measured using the software Meazure (C Thing Software).

The electrical properties of PCL, PCL/GO and PCL/rGO were evaluated via electrical impedance measurements. The experiments were carried out using a PM 6304 programmable automatic RCL meter (Philips) that was connected to an adapted system composed of two

Nickel foils with a contact area of 5x5cm^2, which act as current collector. The dry membrane, used as electrode, was located between the foils. The system was fitted with clamps during measurements, carried out at 100, 1000 and 100000 Hz and at room temperature.

The impedance analysis provided values of impedance modulus (Z) and phase angle (ϕ). The resistivity of the membranes (δ, Ω.cm) and the dielectric permittivity (ε_r) were calculated using the Equations 1 and 2:

$$R=\delta.(l/S) \quad (1)$$

$$C^{*}=(\varepsilon_r).(S/l) \quad (2)$$

Where l is the average thickness of the membrane [15] (9.1x10^{-3} cm for PCL, 8.5x10^{-3} cm for PCL/GO and 9.7x10^{-3} cm for PCL/rGO) and S is the contact area (25 cm^2).

R and C^{*} were calculated from the the real Z' (Ω) and imaginary Z'' (Ω) impedance modulus, respectively as follows (Equations 3 and 4):

$$R=Z'.cos(\phi) \quad (3)$$

$$C^{*}=1/(Z''.sen(\phi).\omega) \quad (4)$$

Being $\omega=2\pi.f$, where f is the frequency applied.

Scaffold preparation for cell culture assays: Membranes were cut into disks of 15 mm in diameter and kept in 24 well plates (Corning). Samples were sterilised by soaking in 70% ethanol for 1 hour and subsequently rinsed three times in PBS (Thermo Fisher). After that, membranes were submerged in a solution of 1% Penicillin-Streptomycin (P/S, Thermo Fisher) in PBS for 6 hours and then washed three times in PBS. Finally, air-dried membranes were exposed to UV light for 20 minutes in a laminar flow cabinet.

Polydimethylsiloxane (PDMS, Dow Corning) rings with an internal diameter of 11 mm were fabricated and placed on the surface of the membranes to keep the membranes from floating and prevent cells from migrating out of the membranes. The final effective surface area of the membranes for cell seeding was 0.95 cm^2. Before seeding, all samples were coated with

diluted Matrigel and incubated for a minimum of four hours. Matrigel dilution was prepared from hESC-qualified Matrigel (Corning) diluted in ice cold KnockOut-DMEM (Thermo Fisher) according to batch-specific manufacturer instructions.

NPC culture for proliferation, differentiation and maturation: All reagents were provided by Thermo Fisher, unless otherwise stated.

NPCs were differentiated from iPSCs, following a dual SMAD inhibition adherent protocol [Bianchi et al, 2018, in preparation]. iPSCs quality control was performed before cryopreservation. Briefly, iPSCs were obtained through StemBANCC, Oxford, and cultured in mTeSR medium (StemCell Technologies) in feeder-free conditions on matrigel-coated well plates. iPSC colonies were passaged at confluency, and used within four passages of thawing. iPSCs were nerualised by small molecule dual-SMAD inhibition, with concurrent Wnt activation and ϒ-secretase inhibition for one week, after which rosettes of SOX1, Pax6 and nestin positive cells, markers of NPC identity, were observed.

For proliferation assays, NPCs were dissociated using Accutase and seeded on the surface of matrigel-coated membranes at a density of 6.6 x 10^4 cells·cm^{-2} in NPC proliferation medium, which was replaced daily. Cell proliferation was evaluated after 5 days. Proliferation medium consisted of 50% KO-DMEM:F12 and 50% Neurobasal Medium, supplemented with 1% P/S, 1% B27, 1% N2, 1% Non Essential Amino Acids, 1% GlutaMAX, 0.1 mM L-Ascorbic Acid (Sigma-Aldrich), 10 ng·mL^{-1} b-Fibroblast Growth Factor (b-FGF) and 10 ng·mL^{-1} Epidermal Growth Factor (EGF, Peprotech).

For neural differentiation assays, NPCs were dissociated using Accutase and seeded on the surface of the membranes at a density of 3.5 x 10^4 cells·cm^{-2} in NPC expansion medium. After day 1, proliferation medium was substituted with differentiation medium. Cells for differentiation analysis were kept for 7 days in differentiation medium, which was replaced daily. Differentiation media consisted of 50% KO-DMEM:F12 and 50% Neurobasal Medium, supplemented with 1% P/S, 0.5% B27, 1% N2, 1% Non-Essential Amino Acids, 1%

GlutaMAX , 0.1mM L-Ascorbic Acid, 10uM All-Trans Retinoic Acid (Sigma Aldrich), 100ng/ml recombinant Sonic Hedgehog (Peprotech), 0.5uM Purmorphamine (Abcam) and 1mM SAG Dihydrochloride (Sigma Aldrich).

For neural maturation, differentiated NPCs were dissociated from six-well plates using Accutase and seeded onto the membranes at a density of 5.5 x 10^4 cells·cm^{-2} in maturation medium for up to 20 days, with daily medium change. Maturation medium consisted of 50% KO-DMEM:F12 and 50% Neurobasal Medium supplemented with 1% P/S, 1% B27, 1%N2, 1% NEAA, 1% GlutaMAX , 0.1 mM L-AA, 10 ng·mL^{-1} CNTF (Peprotech), 10 ng·mL^{-1} BDNF (Peprotech), 10 ng·mL^{-1} NT-3 (Peprotech) and 10 ng·mL^{-1} GDNF (Peprotech).

Cells cultured in 24-well tissue culture plates (TCP) were used as controls for proliferation, differentiation and maturation assays.

Immunocytochemistry and image analysis: Cells on the membranes and TCP plates were fixed using 3.7% Paraformaldehyde solution in PBS (PFA, ≥ 36%, Sigma Aldrich). Fixed cells were permeabilised using a solution of 0.1% Triton-X (Fisher Biotec), 0.1% Tween-20 (Sigma Aldrich), 1% Bovine Serum Albumen (Sigma Aldrich) in PBS. Primary antibody for neural specific beta-III tubulin (Tuj1, AbCam) was added at 1:1000 concentration in a 1:10 dilution of the permeabilisation buffer, and kept overnight at room temperature on a gyro rocker at 5 rpm. Subsequently, AlexaFluor 488 secondary antibody (LifeTechnologies) was added at a concentration of 1:500, and kept in the dark at room temperature for 4 hours on a gyro rocker. Cell nuclei were counterstained with NucBlue (2 drops·mL^{-1} medium).

Widefield Microscopy images of membranes were taken using a Nikon TI-E inverted fluorescence microscope with multi-wavelength LED excitation. Confocal images were taken using a Zeiss LSM-710 confocal microscope. Image analysis was carried out using Fiji (ImageJ) software.

Scanning Electron Microscopy (SEM): SEM images of matured neurons on the membranes were taken at day 20. Samples were prepared by fixing the cells using a solution of 10%

$NaHPO_4$ (Sigma Aldrich), 50% PFA and 10% Glutaraldehide (Sigma Aldrich) in distilled water, adjusted to pH 7.4. Membranes were submerged in the fixation solution for 20 minutes, washed with PBS and dehydrated using progressive concentrations of distilled water/ethanol (>99.8%, Honeywell) from 100/0 to 0/100. SEM imaging was carried out using a Zeiss Sigma 300 FEG-SEM in high-vacuum mode, at an acceleration voltage of 2 kV.

Spontaneous Calcium Activity Recording: Imaging of spontaneous calcium activity was carried out to analyse the neural activity of matured neuons after 20 days. Cells were incubated for 30 minutes in staining solution of 4μM Oregon Green 488 Bapta-1 (Thermo Fisher) in imaging medium (FluoroBrite-DMEM, Thermo Fisher). Cells were then incubated with fresh FB-DMEM medium for 30 minutes before time-lapse videos were recorded at 5 frames per second for 2 minutes, using standard FITC filters .Analysis of calcium imaging was carried out in ImageJ by isolating regions of interest corresponding to cell bodies, and measuring changes in fluorescence intensity in time.

Statistical analysis: Statistical analysis was carried out using GraphPad Prism Software. One-way ANOVA test with Tukey's multiple comparison was used to calculate significant results of contact angle, conductivity measurements and cell culture analysis including proliferation, %Tuj1 expression, length of neurites, number of active neurons and magnitude of cell activity. Significance values were set at $p<0.05$ in all cases. Average values are expressed as mean ± SD, $n\geq3$ for all datasets.

Supporting Information
Supporting Information is available from the Wiley Online Library or from the author.

Acknowledgements: This work was supported by the Cantabria Explora project [JP03.640.69]; the MINECO/AEI and FEDER-Spain project [CTM2016-75509-R], EPSRC [F.B. funding through DTP award number 1514540] and a short-term fellowship from the European Molecular Biology Organization (EMBO) [ref 7189]. Authors would like to thank Dr. Errin Johnson for her assistance with SEM images (performed at the Dunn School EM Facility, Oxford) and the Department of Physical Chemistry of the University of Valencia where the electrical impedance measurements were carried out.

Received: Month XX, XXXX; Revised: Month XX, XXXX; Published online:

((For PPP, use "Accepted: Month XX, XXXX" instead of "Published online")); DOI: 10.1002/marc.((insert number)) ((or ppap., mabi., macp., mame., mren., mats.))

Keywords: graphene oxide, reduced graphene oxide, poly(ε-caprolactone), neural activity, neural stem cell differentiation

[1] R. F. Halliwell, *Neurochem. Int.* **2017**, *106*, 37.

[2] S. Shah, P. T. Yin, T. M. Uehara, S. T. D. Chueng, L. Yang, K. B. Lee, *Adv. Mater.* **2014**, *26*, 3673.

[3] G. Orive, E. Anitua, J. L. Pedraz, D. F. Emerich, *Nat. Rev. Neurosci.* **2009**, *10*, 682.

[4] P. Sensharma, G. Madhumathi, R. D. Jayant, A. K. Jaiswal, *Mater. Sci. Eng. C* **2017**, *77*, 1302.

[5] O. Akhavan, E. Ghaderi, S. A. Shirazian, R. Rahighi, *Carbon N. Y.* **2016**, *97*, 71.

[6] J. Duan, Y. ning Xie, J. hui Yang, T. Huang, N. Zhang, Y. Wang, J. hong Zhang, *Polym. Test.* **2016**, *56*, 220.

[7] Y. Volkov, J. McIntyre, A. Prina-Mello, *2D Mater.* **2017**, *4*, 022001.

[8] Kenry, W. C. Lee, K. P. Loh, C. T. Lim, *Biomaterials* **2018**, *155*, 236.

[9] F. J. O'Brien, *Mater. Today* **2011**, *14*, 88.

[10] S. R. Shin, Y. C. Li, H. L. Jang, P. Khoshakhlagh, M. Akbari, A. Nasajpour, Y. S.

Zhang, A. Tamayol, A. Khademhosseini, *Adv. Drug Deliv. Rev.* **2016**, *105*, 255.

[11] S. Kumar, K. Chatterjee, *ACS Appl. Mater. Interfaces* **2016**, 26431.

[12] M. A. Woodruff, D. W. Hutmacher, *Prog. Polym. Sci.* **2010**, *35*, 1217.

[13] T. Bouzid, A. Sinitskii, J. Y. Lim, *Neural Regen. Res.* **2016**, *11*, 894.

[14] J. Song, H. Gao, G. Zhu, X. Cao, X. Shi, Y. Wang, *Carbon N. Y.* **2015**, *95*, 1039.

[15] N. Diban, S. Sánchez-González, M. Lázaro-Díez, J. Ramos-Vivas, A. Urtiaga, *J. Memb. Sci.* **2017**, *540*, 219.

[16] S. Sánchez-González, N. Diban, A. Urtiaga, *Membranes (Basel).* **2018**, *8*, 1.

[17] O. Akhavan, *J. Mater. Chem. B* **2016**, *4*, 3169.

[18] O. Akhavan, E. Ghaderi, E. Abouei, S. Hatamy, E. Ghasemi, *Carbon N. Y.* **2014**, *66*, 395.

[19] S. Sayyar, E. Murray, B. C. Thompson, S. Gambhir, D. L. Officer, G. G. Wallace, *Carbon N. Y.* **2013**, *52*, 296.

[20] K. Zhang, H. Zheng, S. Liang, C. Gao, *Acta Biomater.* **2016**, *37*, 131.

[21] N. Golafshan, M. Kharaziha, M. Fathi, *Carbon N. Y.* **2017**, *111*, 752.

[22] A. Wesełucha-Birczyńska, M. Świętek, E. Sołtysiak, P. Galiński, Ł. Płachta, K. Piekara, M. Błażewicz, *Analyst* **2015**, *140*, 2311.

[23] M. J. Allen, V. C. Tung, R. B. Kaner, *Chem. Rev.* **2009**, *110*, 132.

[24] D. Chen, H. Feng, J. Li, *Chem. Rev.* **2012**, *112*, 6027.

[25] Z. Xu, J. Zhang, M. Shan, Y. Li, B. Li, J. Niu, B. Zhou, X. Qian, *J. Memb. Sci.* **2014**, *458*, 1.

[26] S. Kumar, S. Raj, E. Kolanthai, A. K. Sood, S. Sampath, K. Chatterjee, *ACS Appl. Mater. Interfaces* **2015**, *7*, 3237.

[27] B. Chaudhuri, D. Bhadra, L. Moroni, K. Pramanik, *Biofabrication* **2015**, *7*, 15009.

[28] S. G. Rotman, Z. Guo, D. W. Grijpma, A. A. Poot, *Polym. Adv. Technol.* **2017**, *28*, 1233.

[29] A. M. Pinto, S. Moreira, I. C. Gonçalves, F. M. Gama, A. M. Mendes, F. D. Magalhães, *Colloids Surfaces B Biointerfaces* **2013**, *104*, 229.

[30] T. Nezakati, A. Tan, A. M. Seifalian, *J. Colloid Interface Sci.* **2014**, *435*, 145.[31] D. S. H. Phung Xuan Thinh, C. Basavajara, Jin Kyoung Kim, *Polym. Compos.* **2012**, 2159.

[32] B.-H. Kim, K. S. Yang, *J. Ind. Eng. Chem.* **2014**, *20*, 3474.

[33] S. Stankovich, D. A. Dikin, R. D. Piner, K. A. Kohlhaas, A. Kleinhammes, Y. Jia, Y. Wu, **2007**, *45*, 1558.

[34] S. Goenka, V. Sant, S. Sant, *J. Control. Release* **2014**, *173*, 75.

[35] J. R. Potts, D. R. Dreyer, C. W. Bielawski, R. S. Ruoff, *Polymer (Guildf).* **2011**, *52*, 5.

[36] P. Fan, L. Wang, J. Yang, F. Chen, M. Zhong, **2012**, *365702*.

[37] Z. He, S. Zhang, Q. Song, W. Li, D. Liu, H. Li, M. Tang, R. Chai, *Colloids Surfaces B Biointerfaces* **2016**, *146*, 442.

[38] W. Wang, G. Caetano, W. S. Ambler, J. J. Blaker, M. A. Frade, P. Mandal, C. Diver, P. Bártolo, *Materials (Basel).* **2016**, *9*, 992.

[39] B. Mammadov, M. Sever, M. O. Guler, A. B. Tekinay, *Biomater. Sci.* **2013**, *1*, 1119.

[40] S. Y. Park, J. Park, S. H. Sim, M. G. Sung, K. S. Kim, B. H. Hong, S. Hong, *Adv. Mater.* **2011**, *23*, H263.

[41] S. Ryu, B.-S. Kim, *Tissue Eng. Regen. Med.* **2013**, *10*, 39.

[42] R. Guo, S. Zhang, M. Xiao, F. Qian, Z. He, D. Li, X. Zhang, H. Li, X. Yang, M. Wang, R. Chai, M. Tang, *Biomaterials* **2016**, *106*, 193.

[43] P. Ribao, M. J. Rivero, I. Ortiz, *Environ. Sci. Pollut. Res.* **2017**, *24*, 12628.

[44] B. Gomez-Ruiz, P. Ribao, N. Diban, M. J. Rivero, I. Ortiz, A. Urtiaga, *J. Hazard. Mater.* **2018**, *344*, 950.

[45] O. Akhavan, *Carbon N. Y.* **2014**, *81*, 158.

1
2

The table of contents

The oxidative state of graphene-based nanomaterials in composite poly(ε-caprolactone) membranes affects the differentiation and electrophysiological response at maturation of human iPSC-derived neural progenitor cells**.** Nanomaterials polarity induces different phase separation and distribution into the membrane matrix**.** Albeit reduced graphene oxide is embedded in the membrane center, significant improvement on the differentiation and magnitude of activity spikes of neurons was observed.

Keywords

graphene oxide, reduced graphene oxide, poly(ε-caprolactone), neural activity, neural stem cell differentiation

Sandra Sánchez-González, Nazely Diban*, Fabio Bianchi, Hua Ye, Ane Urtiaga

Evidences of the Effect of GO and rGO in PCL Membranes on the Differentiation and Maturation of Human Neural Progenitor Cells

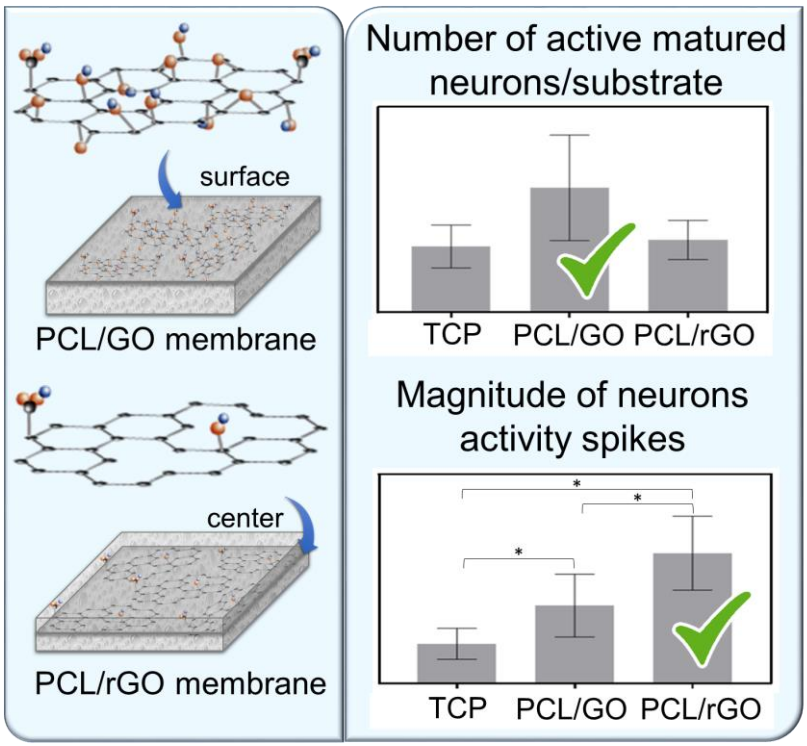

Supporting Information

Evidences of the Effect of GO and rGO in PCL Membranes on the Differentiation and Maturation of Human Neural Progenitor Cells

Sandra Sánchez-González, Nazely Diban*, Fabio Bianchi, Hua Ye, Ane Urtiaga

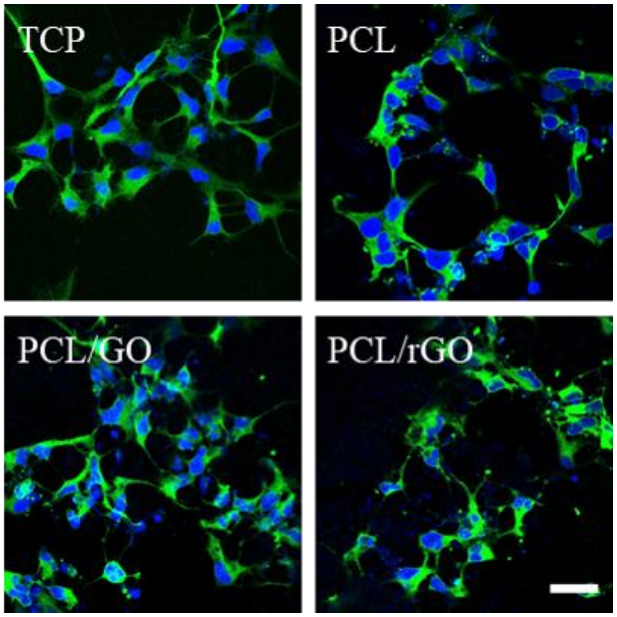

Figure S1. Confocal images of NPCs adhered on TCP, PCL, PCL/GO and PCL/rGO samples after day 1. The nuclei and the plasma membrane of NPCs were stained by nuc-blue (blue) and Tuj1 (green), respectively. Scale bar = 50 µm.

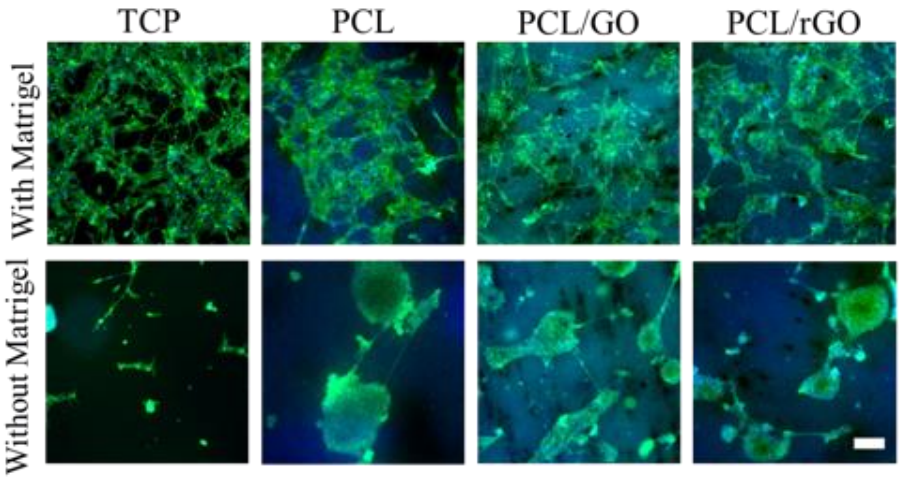

Figure S2. Fluorescence images of NPC cultured on Matrigel-coated and non-coated substrates after day 1. NPC cultured on non-coated substrates caused cluster formations of cells, while the cells on Matrigel-coated substrates spread out and homogeneous. The cell

attachment was reduced for non-coated samples. Scale bar = 100 μm.